Segmentation of hippocampal subregion via 5-Tesla magnetic resonance imaging: a comparative study

Lixian Zou[1], Yijun Zhou[2], Shuo Chen[3], Jun Ni[4], Ye Li[1,5], Dong Liang[1,5], Xin Liu[1,5,6], Yining Wang[2#], Hairong Zheng[1,5#]

[1]Paul C. Lauterbur Research Center for Biomedical Imaging, Shenzhen Institute of Advanced Technology, Chinese Academy of Science, Shenzhen, China; [2]Department of Radiology, State Key Laboratory of Complex Severe and Rare Diseases, Peking Union Medical College Hospital, Chinese Academy of Medical Sciences and Peking Union Medical College, Beijing, China; [3]United Imaging Healthcare Co., Ltd., Shanghai, China; [4]Department of Neurology, Peking Union Medical College Hospital, Chinese Academy of Medical Sciences and Peking Union Medical College, Beijing, China; [5]Key Laboratory for Magnetic Resonance and Multimodality Imaging of Guangdong Province, Shenzhen, China; [6]Faculty of Biomedical Engineering, Shenzhen University of Advanced Technology, Shenzhen, China

Contributions: (I) Conception and design: L Zou, Y Wang, H Zheng; (II) Administrative support: Y Li, D Liang; (III) Provision of study materials or patients: S Chen, X Liu, H Zheng; (IV) Collection and assembly of data: L Zou, Y Zhou; (V) Data analysis and interpretation: L Zou, J Ni, Y Wang; (VI) Manuscript writing: All authors; (VII) Final approval of manuscript: All authors.

[#]These authors contributed equally to this work.

Correspondence to: Yining Wang, MD. Department of Radiology, State Key Laboratory of Complex Severe and Rare Diseases, Peking Union Medical College Hospital, Chinese Academy of Medical Sciences and Peking Union Medical College, No. 1 Shuaifuyuan Wangfujing, Dongcheng District, Beijing 100730, China. Email: wangyining@pumch.cn; Hairong Zheng, PhD. Paul C. Lauterbur Research Centre for Biomedical Imaging, Shenzhen Institute of Advanced Technology, Chinese Academy of Sciences, No. 1068 Xueyuan Avenue, Shenzhen University Town, Xili, Nanshan District, Shenzhen 518055, China; Key Laboratory for Magnetic Resonance and Multimodality Imaging of Guangdong Province, No. 1068 Xueyuan Avenue, Shenzhen University Town, Xili, Nanshan District, Shenzhen 518055, China; National Innovation Center for Advanced Medical Devices, No. 53 Liuxian Avenue, Longhua District, Shenzhen 518110, China. Email: hr.zheng@siat.ac.cn.

Background: Small voxel sizes in two-dimensional (2D) hippocampal magnetic resonance imaging (MRI) facilitate subfield segmentation. However, thinner slices remain challenging despite the advancements in in-plane resolution due to the tradeoffs in image quality. A higher signal-to-noise ratio (SNR) at 5 Tesla (T) compared to 3 T could enable thinner slices; however, the effects of changes in tissue contrast and inhomogeneous B1 variation may be weaken the SNR and contrast-to-noise ratio (CNR). However, the effectiveness of current automatic segmentation tools in handling 5-T images, particularly for thinner slices, remains to be fully elucidated. This study thus aimed to assess hippocampus image quality improvement from 3 to 5 T and to evaluate the autosegmentation of the hippocampal subregion on 5 T with different slice thicknesses.

Methods: This prospective study included 28 healthy participants (14 females, with a mean age of 31.8±8.96 years). T2-weighted series with 2-, 1-, and 0.7-mm slice thicknesses were acquired on 3 T and 5 T. CNR, SNR, and visual scores of the molecular layer were compared. Hippocampal subregions were segmented with 5-T data using FreeSurfer and HippUnfold toolboxes. Dice coefficients of stratum radiatum, lacunosum, and moleculare (SRLM) were compared between FreeSurfer and HippUnfold. Fleiss' Kappa, the Kruskal-Wallis test, and the pairwise Wilcoxon signed-rank test were used for statistical analyses, with a P value <0.05 being considered statistically significant.

Results: SNR, CNR, and visual scores were higher on 5 T than on 3 T at the same slice thickness. The SNR of the 1-mm T2 images on 5 T was comparable to that of 2-mm images on 3 T, and the CNR of the 0.7-mm images on 5 T was comparable to that of the 2-mm images on 3 T. With a reduction in slice

thickness, the Dice coefficients of SRLM between HippUnfold and manual segmentation increased, while those between FreeSurfer and manual segmentation decreased.

Conclusions: The 5-T magnetic resonance system offers higher SNR and CNR values for hippocampal imaging as compared to 3-T imaging. A slice thickness of 0.7–1 mm is recommended for 2D T2-weighted imaging. However, in the selection of automatic segmentation tools for hippocampal subregions, caution is advised if the slice thickness is less than 2 mm.

Keywords: Magnetic resonance imaging (MRI); brain; hippocampus; hippocampal subregions; ultrahigh field

Introduction

The hippocampus is composed of several interacting subfields with different cytoarchitectures and functions (1) and plays a crucial role in memory formation (2,3), learning processes (4), and spatial navigation (5). It can be affected by a broad range of neuropsychiatric disorders (6-10), such as Alzheimer disease, temporal lobe epilepsy, hippocampal sclerosis, and psychosis. In particular, alternations in hippocampal subfields are selectively linked to subtypes of diseases (10-12), suggesting that subfield analysis may provide critical biomarkers for understanding cognitive process and their disruption in neurological disorders.

Numerous *in vivo* studies have assessed subfield volumes of the hippocampal formation through magnetic resonance imaging (MRI) (13-15). Manual segmentation is the gold standard for identifying hippocampal subfields in MRI, offering precise delineation based on the geometric relationships between substructures (16). However, this approach is labor-intensive and time-consuming, prompting the adoption of automated segmentation tools (17-21), such as FreeSurfer (20) and HippUnfold (21). These tools facilitate efficient and reproducible hippocampal subfield segmentation; however, despite their advantages, there are discrepancies in the segmentation outcomes across different tools (22), highlighting the need for standardized subregional definitions and protocols (23). In the Alzheimer's Disease Neuroimaging Initiative 2 (ADNI2) study, high-resolution T2-weighted hippocampal images outperformed T1-weighted imaging in subfield segmentation (22). Additionally, it has been reported that the stratum radiatum, lacunosum, and moleculare (SRLM), a thin structural feature visible as a hypointense band on T2-weighted imaging, can serve as a crucial boundary for

hippocampal subfield segmentation (24,25).

The bulk of studies on the hippocampus have used two-dimensional (2D) T2-weighted imaging with high in-plane resolution, typically 0.4 mm × 0.4 mm (25-27). However, the slice thickness (or through-plane resolution) of 2D T2-weighted imaging, a parameter critical for the precise segmentation of the subtle hippocampal subarchitectures such as the SRLM, has not been extensively examined in the context of hippocampal subfield segmentation. This is partly due to the insufficient signal-to-noise ratio (SNR) of conventional 3-Tesla (T) MRI. Ultrahigh magnetic fields, such as 5 T and beyond, provide superior SNR, potentially enhancing hippocampal subfield segmentation by improving spatial resolution and tissue contrast. An increased SNR facilitates higher image quality and spatial resolution (28), enabling precise delineation of hippocampal subfields. Meanwhile, enhanced tissue contrast improves effective differentiation, offering greater segmentation accuracy and reliability. Although the increased magnetic field strength of 5 T may provide higher image quality, the benefits of hippocampal subfield segmentation remain worth exploring, as the risks associated with a higher field, such as B1 inhomogeneity and T2 shortening effect, remain uncertain.

In this study, we first compared 5-T MRI and 3-T MRI in their ability to improve the image quality of structures near the hippocampus, with a focus on parameters such as SNR, contrast-to-noise ratio (CNR), and the visual clarity of hippocampal structures. Subsequently, the effectiveness of FreeSurfer and HippUnfold in segmenting the SRLM was evaluated under different slice thicknesses of T2-weighted imaging at 5 T. We present this article in accordance with the STROBE reporting checklist (available at https://qims.amegroups.com/article/view/10.21037/qims-24-2169/rc).

Table 1 Scanning parameters of all protocols

Scanning parameters	2D T2-weighted FSE			3D T1-weighted MPRAGE (5 T)
	T2$_L$	T2$_M$	T2$_H$	
FA	90°			9°
FOV	180 mm × 180 mm × 56 mm			220 mm × 220 mm × 200 mm
Spatial resolution	0.45 mm × 0.45 mm			0.7 mm × 0.7 mm × 0.7 mm
Slice thickness	2 mm	1 mm	0.7 mm	–
TR				
5 T	6,199 ms	12,510 ms	17,832 ms	9.1 ms
3 T	6,456 ms	13,057 ms	18,192 ms	
TE				
5 T	107.7 ms	108.6 ms	94.8 ms	3.2 ms
3 T	98 ms	99.26 ms	98.56 ms	
TA				
5 T	3 min 25 sec	6 min 53 sec	9 min 49 sec	5 min 29 sec
3 T	3 min 33 sec	7 min 11 sec	10 min 01 sec	

T2$_H$, T2$_M$, and T2$_L$: T2-weighted images with slice thickness of 0.7, 1, and 2 mm, respectively. 2D, two-dimensional; 3D, three-dimensional; FSE, fast spin echo; FA, flip angle; FOV, field of view; MPRAGE, magnetization-prepared rapid acquisition of gradient echo; TR, repetition time; TE, echo time; TA, acquisition time.

Methods

Participants

This study was conducted in accordance with the Declaration of Helsinki (as revised in 2013) and approved by the institutional ethics committee of Shenzhen Institute of Advanced Technology, Chinese Academy of Sciences (No. SIAT-IRB-230928-H0673). Written informed consent was obtained from all participants. A total of 28 healthy participants (14 females; mean age 31.8±8.96 years) were recruited from 2023 to 2024 for experiments conducted on a 5-T scanner. Among them, five (two females; mean age 26.6±3.65 years) also underwent additional imaging on a 3-T scanner for image quality comparison with 5-T images. The inclusion criteria for healthy volunteers included (I) age >18 years old, (II) no contraindications to MRI scans, and (III) no history of cardiovascular diseases, head injury, brain surgery, or psychiatric diseases.

Data acquisition

All MRI scans were performed on a 5-T MR scanner (uMR Jupiter, United Imaging Healthcare, Shanghai, China)

with a 2-channel transmit and a 48-channel receive head coil or on a 3-T MR scanner (uMR790, United Imaging Healthcare) with a 32-channel head-and-neck receive-only coil. The MRI protocols consisted of 3D whole-brain T1-weighted imaging and 2D high-resolution T2-weighted imaging. The T1-weighted images were acquired in the sagittal plane with the 3D magnetization-prepared rapid acquisition of gradient echo (MPRAGE) sequence; meanwhile, the T2-weighted images were acquired in an oblique coronal plane orthogonal to the long axis of the hippocampus using a fast-spin-echo (FSE) sequence with three slice thicknesses: 2 mm (T2$_L$), 1 mm (T2$_M$), and 0.7 mm (T2$_H$). The scanning parameters are listed on *Table 1*.

Hippocampal subregion segmentation

Hippocampal subregions were segmented using two methods: the open-source toolbox FreeSurfer 7.2.0 (https://surfer.nmr.mgh.harvard.edu) and the HippUnfold segmentation method (21). For FreeSurfer, each participant was scanned at 5 T, and T1-weighted and T2-weighted images were used as input for subregion segmentation; meanwhile, the use of HippUnfold relied solely on T2-

weighted images. To provide a reference for the evaluation of the segmentation results, the SRLM (also known as the *molecular layer*) was also manually delineated by a toolbox (FSLeyes https://open.win.ox.ac.uk/pages/fsl/fsleyes/fsleyes/userdoc/install.html) based on FSL (FMRIB Software Library) (https://fsl.fmrib.ox.ac.uk/fsl/docs/#/). Specifically, manual segmentation was performed on 0.7-mm T2-weighted images due to their capacity to capture the complex curvatures of the hippocampus. The segmentation process began with the identification of the hippocampal contour in the sagittal plane. Subsequently, the slice with the anterior edge of the hippocampus was designated as the starting point, and the slice containing the posterior edge was designated as the end point. Finally, the SRLM, known as the low-signal "dark band", was manually delineated in the short-axis view via FSLeyes.

Evaluation metrics

The image quality of the T2-weighted FSE sequence was visually assessed by scoring the visualization of the hippocampal internal architecture on T2-weighted images (T2$_L$, T2$_M$, and T2$_H$), which is crucial for hippocampal subregion segmentation. A total of 30 T2-weighted images, scanned on 3-T and 5-T MRI at three slice thicknesses among 5 participants, were initially randomized and evaluated using FreeView (FreeSurfer toolkit) by three independent raters: two experienced neuroradiologists (>3 years of experience) and one neuroradiologist (1 year of experience). Assessment prioritized two anatomical features critical for subregion segmentation: continuity of the molecular layer's hypointense band and boundary sharpness between hippocampal subfields. A validated four-point rating scale (29,30) was employed as follows: a score of 4 indicated complete continuity and clarity of the molecular layer, 3 indicated predominantly continuous visualization of the hypointense band with minor discontinuities, 2 indicated partial visualization of the hypointense band; and 1 indicated little or no discernible molecular layer. The in-plane (coronal) and through-plane (sagittal) image qualities were each scored. *Figure 1* presents examples of the rating scores. The interrater reliability of three readers was evaluated, and for cases with scoring discrepancies, final visual scores were determined via discussion.

The SNR and CNR of T2-weighted images were compared between 3- and 5-T images in the five participants. Given that parallel imaging acceleration in T2-weighted acquisitions fundamentally modifies background

noise characteristics (31,32), SNR and CNR (14) of the hippocampus were qualitatively calculated with following formulae:

$$SNR = \frac{\overline{Signal_{hipp}}}{\sigma_{wm}} \qquad [1]$$

$$CNR = \frac{\left|\overline{Signal_{hipp}} - \overline{Signal_{wm}}\right|}{\sqrt{\sigma_{hipp}^2 + \sigma_{wm}^2}} \qquad [2]$$

where $\overline{Signal_{hipp}}$ and $\overline{Signal_{wm}}$ are the mean signal intensities in hippocampal gray matter and uniform white-matter region near the hippocampus, respectively; and σ_{wm} and σ_{hipp} are the standard deviation of the white matter and hippocampus, respectively.

Manual segmentation of the SRLM served as the reference standard for evaluating the automated segmentation outcomes. Segmentation accuracy was evaluated via the Dice coefficient. All images and segmentation results were registered to T2-weighted images with a 0.7-mm slice thickness. Subsequently, the Dice coefficient was calculated as follows:

$$DICE_{auto,manual} = \frac{\left|SRLM_{auto} \cap SRLM_{manual}\right|}{\left(\left|SRLM_{auto}\right| + \left|SRLM_{manual}\right|\right)/2} \qquad [3]$$

where $SRLM_{auto}$ and $SRLM_{manual}$ are the binary masks of the SRLM from the automated segmentation method (FreeSurfer or HippUnfold) and manual segmentation, respectively. The Dice coefficient would be 1 if the SRLM was ideally positioned, <1 if the overlap was less than ideal, and 0 if there is no overlap at all.

Statistical analysis

Statistical analyses were performed in Python 3.2 (https://www.python.org; Python Software Foundation, Wilmington, DE, USA) and SPSS software (IBM Corp., Armonk, NY, USA). The Wilcoxon signed-rank test was used to compare CNR, SNR and image qualities between the 3- and 5-T images for each slice thickness. For comparisons across three slice thicknesses within each magnetic field strength, Kruskal-Wallis with Bonferroni-corrected pairwise analyses were implemented. Interrater reliability of three readers was evaluated via Fleiss's kappa. The Dice coefficients for SRLM between automated segmentation methods and among the three different slice thickness were compared using the Wilcoxon signed-rank
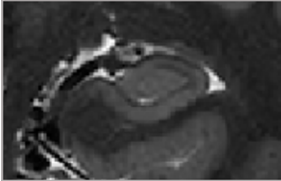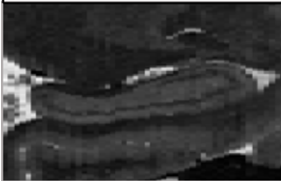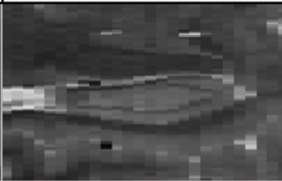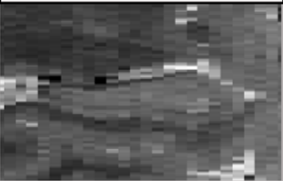
Figure 1 Description of the hippocampus rating criteria. The images show examples of each of the four scoring levels.

test and the Kruskal-Wallis test with Bonferroni correction, respectively. A two-sided P value of <0.05 was considered significant.

Results

Superior visualization of hippocampal internal architecture was consistently achieved at 5 T across all slice thicknesses, with significant improvements in anatomical delineation being particularly evident in thinner slices (*Figure 2*). Results of visual image quality assessment on T2-weighted images with three different thicknesses are shown in *Figure 3*. Notably, no rating score of 1 was found in any of the 5-T images with interrater agreement reaching substantial reliability (Fleiss' κ: in-plane left =0.757, in-plane right =0.695, through-plane left =0.745, in-plane right =0.818). Compared to thicker slices, thinner slices demonstrated

enhanced through-plane continuity due to lower partial volume effects, as illustrated in *Figure 4*.

Quantitative analyses revealed significant field strength advantages despite SNR and CNR reductions with decreasing slice thickness in T2-weighted images, with the CNR and SNR on 5 T being much higher than that on 3T (P=0.043) (*Figure 5* and *Table 2*). Specifically, CNR of images with a 0.7-mm slice thickness on 5 T was comparable to those of images with a 2-mm thickness; meanwhile, the SNR of images with a 1-mm slick thickness on 5 T were comparable to those with a 2-mm thickness on 3 T. The Kruskal-Wallis test confirmed strong slice thickness dependence for SNR at 3 T (left: P=0.004; right: P=0.002) and 5 T (left: P=0.004; right: P=0.004) and for CNR at 3 T (left P=0.005; right P=0.002) and 5 T (left P=0.006; right P=0.002). Additionally, pairwise comparisons with the Bonferroni correction demonstrated a significant

3866

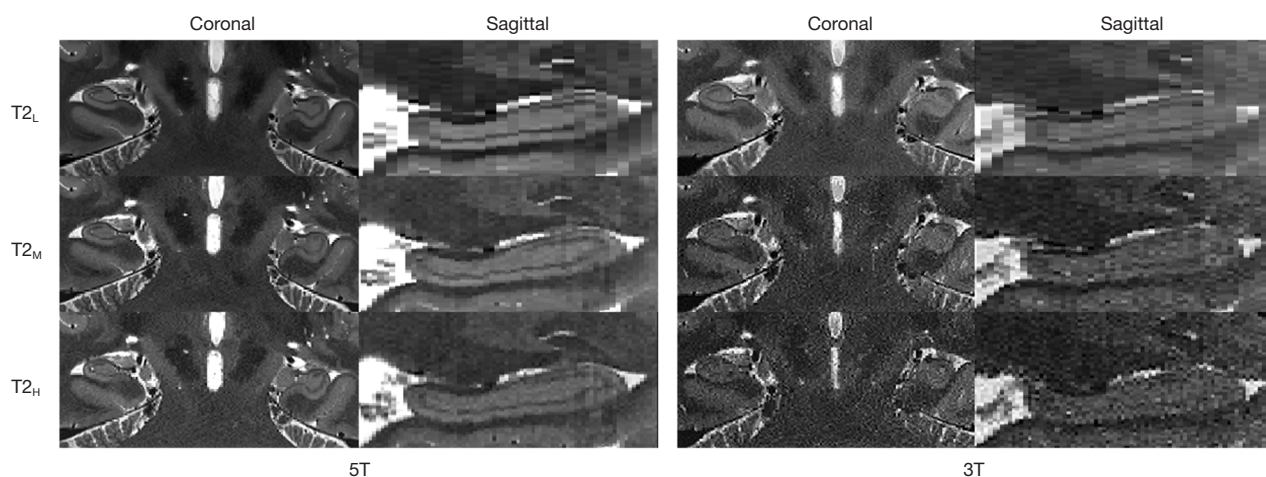Zou et al. Segmentation of hippocampal subregion via 5-T MRI

Figure 2 Illustration of differences in image quality and internal architecture clarity between images with different thicknesses at 3 and 5 T in a single participant. The two panels show that the image quality improves with the increasing intensity of the magnetic field, especially at a submillimeter slice thickness.
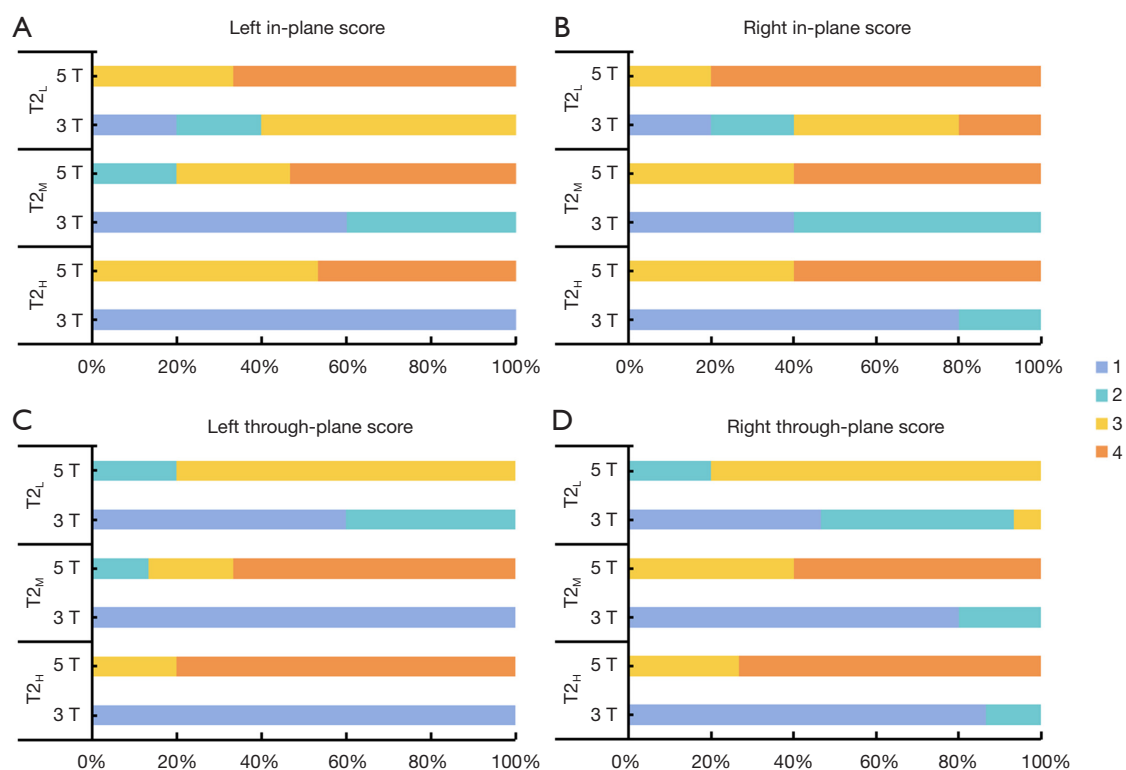

Figure 3 Image quality comparison between different slice thicknesses of T2-weighted images on 3 and 5 T. (A,B) In-plane visualization scores for the left and right hippocampi. (C,D) Through-plane visualization scores for bilateral hippocampi. Visual scores were rated by three readers for all five participants. 4-point scale: 4= excellent molecular layer continuity/clarity, 3= good, 2= limited, and 1= nondiagnostic. $T2_H$, $T2_M$, and $T2_L$: T2-weighted images with a slice thickness of 0.7, 1, and 2 mm, respectively.
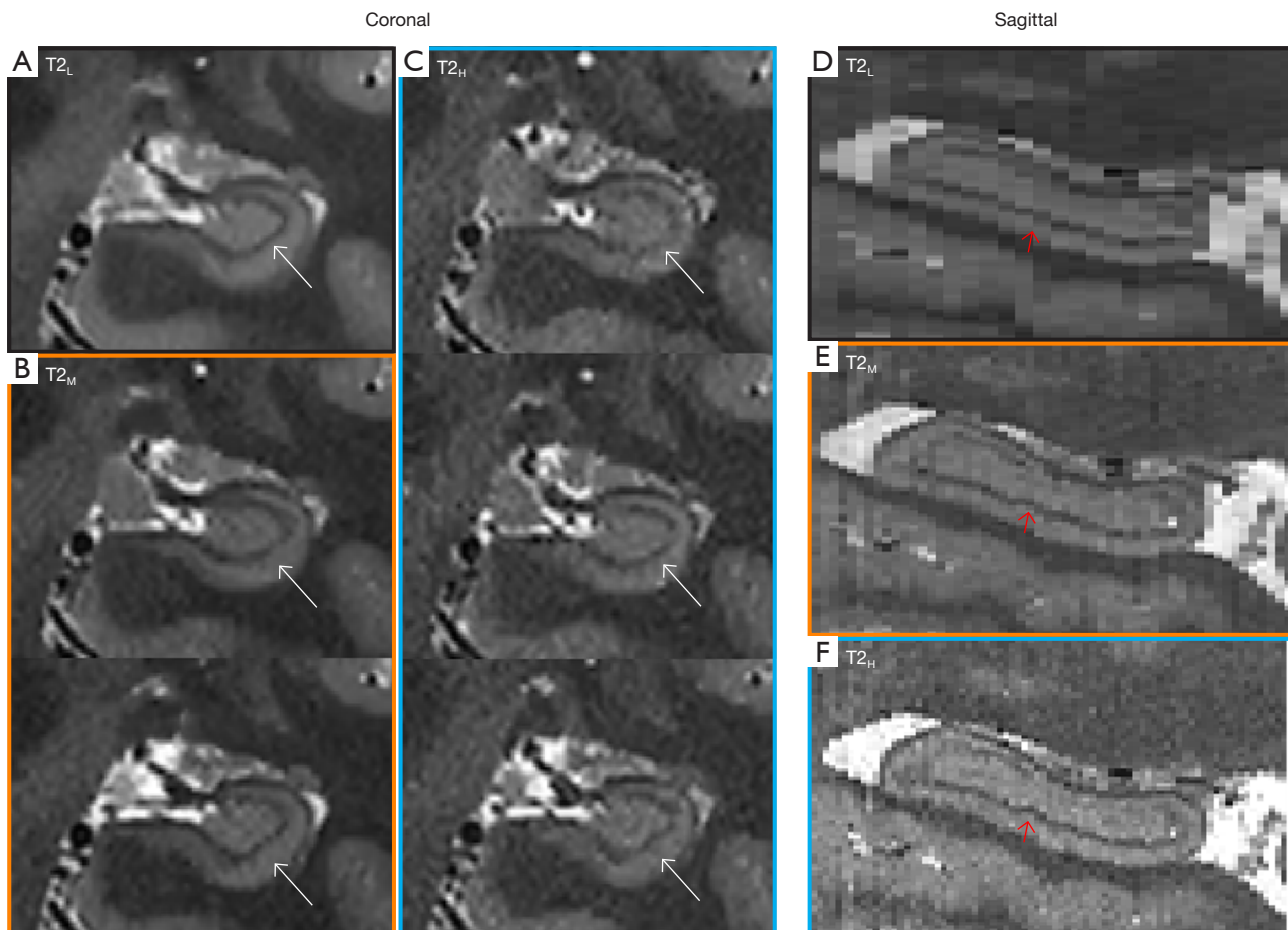
Figure 4 Partial volume effect in the slice direction. (A-C) Coronal plane comparison: 2-mm single slice (A) versus composite 1- (B) and 0.7-mm (C) acquisitions spanning equivalent 2-mm volumes. The white arrows show that the contour of the SRLM varied significantly from slice to slice in the inferolateral aspect of the hippocampus, which resulted in blurring in that portion of the SRLM in (A) due to volume averaging. (D-F) Sagittal plane counterparts reveal thickness-dependent SRLM definition preservation (red arrows indicate the microstructural transitions in 0.7-mm slices and the smoothing artifacts in 2-mm slices). $T2_H$, $T2_M$, and $T2_L$: T2-weighted images with a slice thickness of 0.7, 1, and 2 mm, respectively. SRLM, stratum radiatum, lacunosum, and moleculare.

difference between the $T2_H$ and $T2_L$ slice thicknesses in terms of CNR on 3 T (left: P=0.001; right: P=0.001) and 5 T (CNR: left: P=0.006; right: P=0.004) and SNR at 3 T (left: P=0.003, right: P=0.001) and 5T (SNR: left: P=0.003, right: P=0.003).

Comparative analysis of SRLM segmentation performance across the automation pipelines (HippUnfold *vs.* FreeSurfer) and manual labeling indicated protocol-dependent variations in a representative 5-T scan (n=28 participants; *Figure 6*). Both automated tools performed well in segmenting the hippocampal body but did less well in the hippocampal head as compared to manual labeling. Visual segmentation improvements occurred with a thinner

slice thickness. For FreeSurfer versus manual delineation, the $DICE_{FS,manual}$ for $T2_L$, $T2_M$, and $T2_H$ were 0.59, 0.54, and 0.52 in the left hippocampus, respectively, while in the right hippocampus, they were 0.64, 0.59, and 0.58, respectively (*Figure 7*). The Dice coefficients between HippUnfold and manual segmentation ($DICE_{HU,manual}$) for $T2_L$, $T2_M$, and $T2_H$ were 0.72, 074, and 0.78 on the left side, respectively, while they were 0.70, 0.73, and 0.76 on the right side, respectively.

The Kruskal-Wallis test showed significant differences between the three T2 series on both $DICE_{FS,manual}$ (left: P=0.025; right: P=0.001) and $DICE_{HU,manual}$ (left: P<0.001; right: P<0.001). As indicated in *Table 3*, pairwise comparisons with Bonferroni correction indicated significant differences

3868

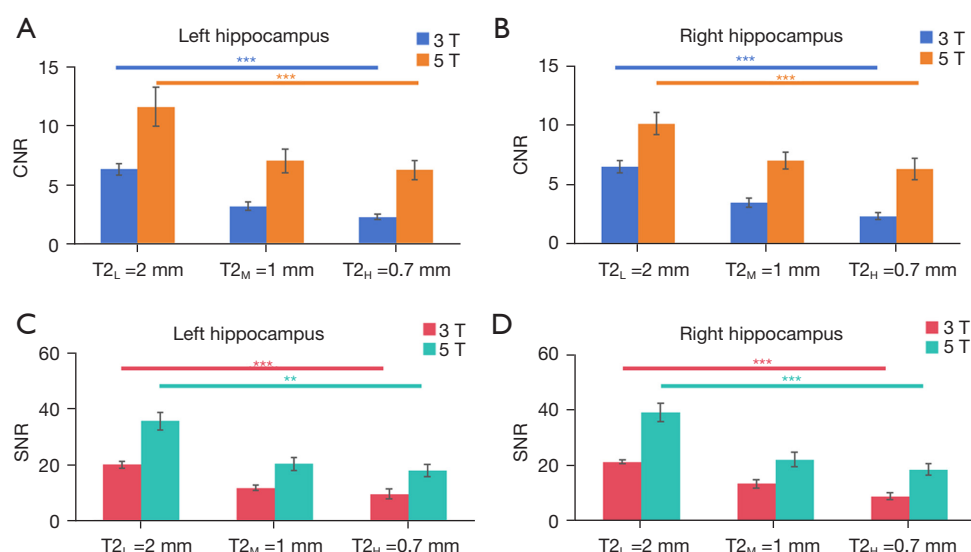Zou et al. Segmentation of hippocampal subregion via 5-T MRI

Figure 5 Comparison of CNR and SNR of T2-weighted images with different slice thicknesses on 3 and 5 T. Error bars represent a standard deviation above and below the mean. **, $P<0.01$; ***, $P<0.005$. CNR, contrast-to-noise ratio; SNR, signal-to-noise ratio.

Table 2 CNR and SNR of T2-weighted images (mean ± standard deviation)

Protocol	CNR		SNR	
	3 T	5 T	3 T	5 T
T2$_L$				
Left	6.30±0.48	11.56±1.63	20.24±1.25	35.77±3.14
Right	6.46±0.51	10.09±0.93	21.32±0.71	39.05±3.22
T2$_M$				
Left	3.17±0.35	7.01±0.99	11.93±0.96	20.52±2.33
Right	3.49±0.37	7.00±0.71	13.50±1.41	22.16±2.61
T2$_H$				
Left	2.30±0.24	6.23±0.79	9.78±1.66	18.16±2.17
Right	2.36±0.29	6.29±0.88	9.07±1.25	18.58±2.04

T2$_H$, T2$_M$, and T2$_L$: T2-weighted images with slice thickness of 0.7, 1, and 2 mm, respectively. CNR, contrast-to-noise ratio; SNR, signal-to-noise ratio.

between the T2$_H$ and T2$_L$ slice thicknesses for both FreeSurfer (left: $P=0.023$; right: $P=0.001$) and HippUnfold (left: $P<0.001$; right: $P<0.001$). Additionally, significant differences were also found between T2$_M$ and T2$_L$ at $DICE_{FS,manual}$ of the right hippocampus ($P=0.007$) and between T2$_M$ and T2$_H$ at $DICE_{HU,manual}$ (left: $P<0.001$; right: $P=0.004$). *Figure 8* illustrates the different hippocampal subregions segmented with FreeSurfer and HippUnfold in the same participant.

Discussion

This study examined the enhancement of hippocampal image quality on 5-T MRI as compared to that on 3-T MRI while assessing the performance of FreeSurfer and HippUnfold in SRLM segmentation across varying slice thicknesses of T2-weighted imaging at 5 T. The results indicate that higher magnetic fields significantly improve image quality, enabling acquisition of thinner T2-weighted
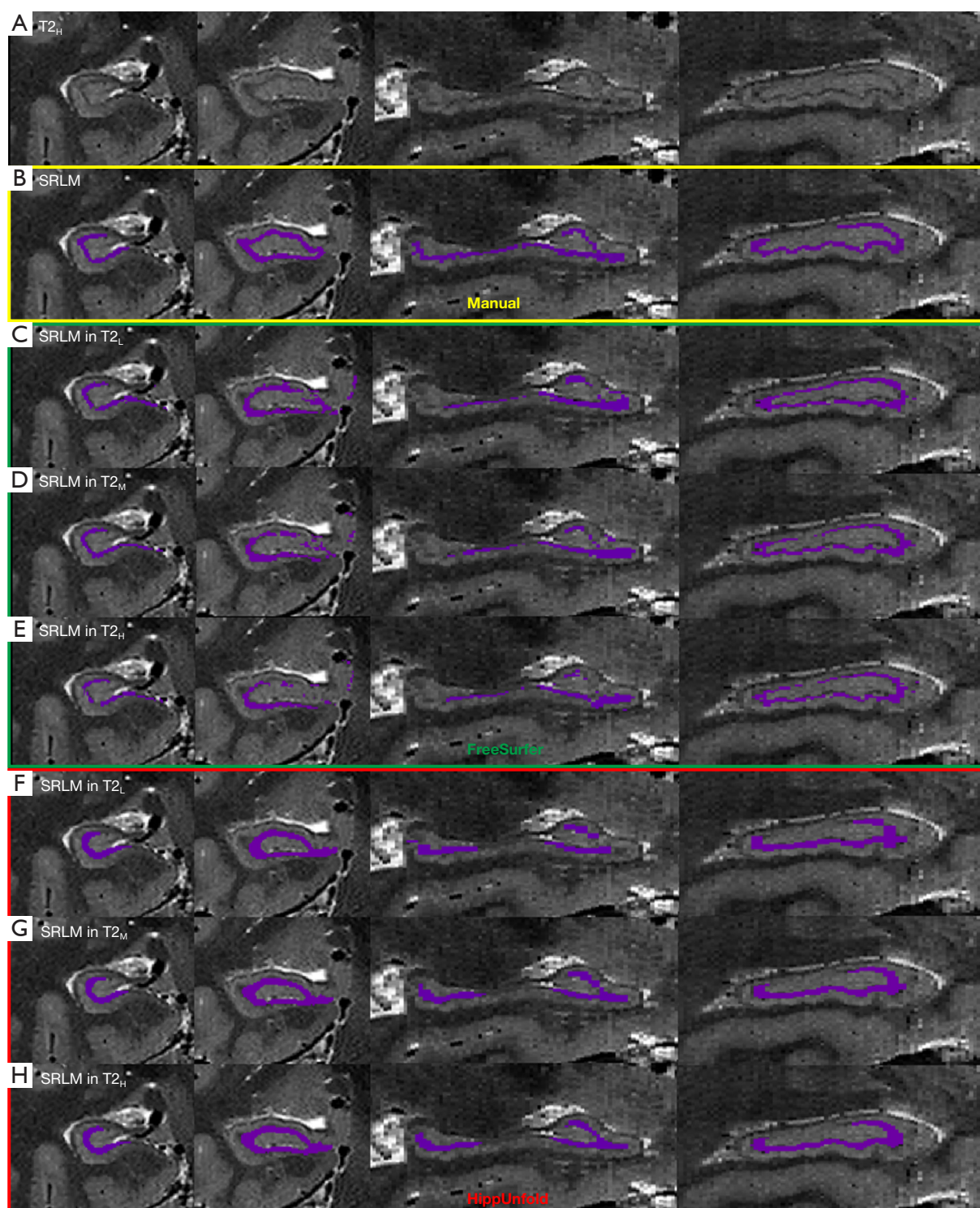
Figure 6 Comparison of the SRLM between HippUnfold, FreeSurfer, and manual demarcation on 5 T. Sagittal and coronal slices are shown for one representative participant. (A) A representative slice of T2-weighted images with a 0.7-mm slice thickness from coronal and sagittal views. These are the base images for (B-H). (B) Manual SRLM delineation: expert-annotated ground truth. (C-E) SRLM in $T2_L$, $T2_M$, and $T2_H$ from FreeSurfer (green). (F-H) SRLM in $T2_L$, $T2_M$, and $T2_H$ from HippUnfold (red). $T2_H$, $T2_M$, and $T2_L$: T2-weighted images with a slice thickness of 0.7, 1, and 2 mm, respectively. SRLM, stratum radiatum, lacunosum, and moleculare.

slices. However, thinner slices do not necessarily imply that all the results from autosegmentation tools will be superior. These findings provide valuable insights for tool improvement and guidance for future research, underlining the significance of thin slices in accurately segmenting hippocampal substructures.

Comparative analysis showed that 5-T T2-weighted imaging exhibited higher SNR, CNR, and visual image quality as compared to 3-T imaging. The improved SNR facilitates the attainment of thinner slice thicknesses in T2-weighted imaging. In our study, we successfully obtained high-resolution T2-weighted images with an outstanding 0.7-mm slice thickness on 5 T, enabling clear visualization of the SRLM of the hippocampus, particularly from the
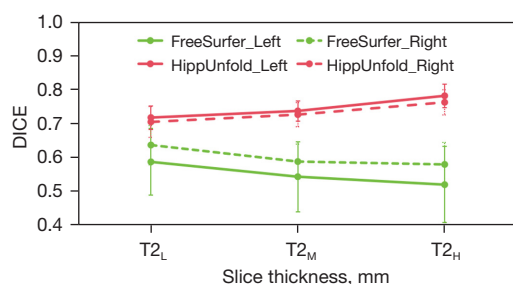

Figure 7 Dice coefficients of the SRLM between the automated and manual segmentation. Error bars represent a standard deviation above and below the mean. $T2_H$, $T2_M$, and $T2_L$: T2-weighted images with slice thickness of 0.7, 1, and 2 mm, respectively. SRLM, stratum radiatum, lacunosum, and moleculare.

through-plane direction. However, this slice thickness at 3 T yielded a no-diagnostic delineation for the SRLM. To visualize the SRLM on 3 T with such a thin slice thickness, methods to mitigate its relatively lower SNR, such as via multiacquisition averaging (30), high-performance coils (33,34), and advanced reconstruction algorithms including artificial intelligence (AI)-assisted compressed sensing (35), could be used at the cost of longer imaging time or greater expense. Moreover, 3D imaging techniques such as sampling perfection with application optimized contrasts using different flip-angle evolutions (SPACE) (14) can provide enhanced resolution in all three dimensions, which might be advantageous for more precise visualization and segmentation of hippocampal subfields.

The discrimination of hippocampal structures demands a small voxel size of images due to the thin structure of the hippocampus. The molecular layer, an internal region of the hippocampus easily recognized on T2-weighted images, serves as a critical anatomical landmark for manual subfield demarcation. Although the in-plane resolution of 2D T2-weighted images can reach up to 0.4 mm, the majority of T2 slice thicknesses are thick, usually 2 mm. Thick slices may obscure fine details, causing segmentation errors via signal averaging. Our results indicated that the enhanced SNR and CNR at 5 T allow for clearer visualization of the internal hippocampal structures, especially the SRLM, even at a 0.7-mm slice thickness. Thinner slices mitigate partial volume effects, augment the visibility of in-plane subfield boundaries, and enhance through-plane SRLM continuity, thus aligning more closely with the integrity

Table 3 Pairwise comparison between Dice coefficients of different slice thicknesses with Bonferroni correction

Group	FreeSurfer		HippUnfold	
	P value	Adjusted P value	P value	Adjusted P value
$T2_H$, $T2_M$				
Left	0.393	>0.99	<0.001	<0.001
Right	0.638	>0.99	0.001	0.004
$T2_H$, $T2_L$				
Left	0.008	0.023	<0.001	<0.001
Right	<0.001	0.001	<0.001	<0.001
$T2_M$, $T2_L$				
Left	0.071	0.212	0.092	0.275
Right	0.002	0.007	0.171	0.512

$T2_H$, $T2_M$, and $T2_L$: T2-weighted images with a slice thickness of 0.7, 1, and 2 mm, respectively. $P < 0.05$ was considered significant.
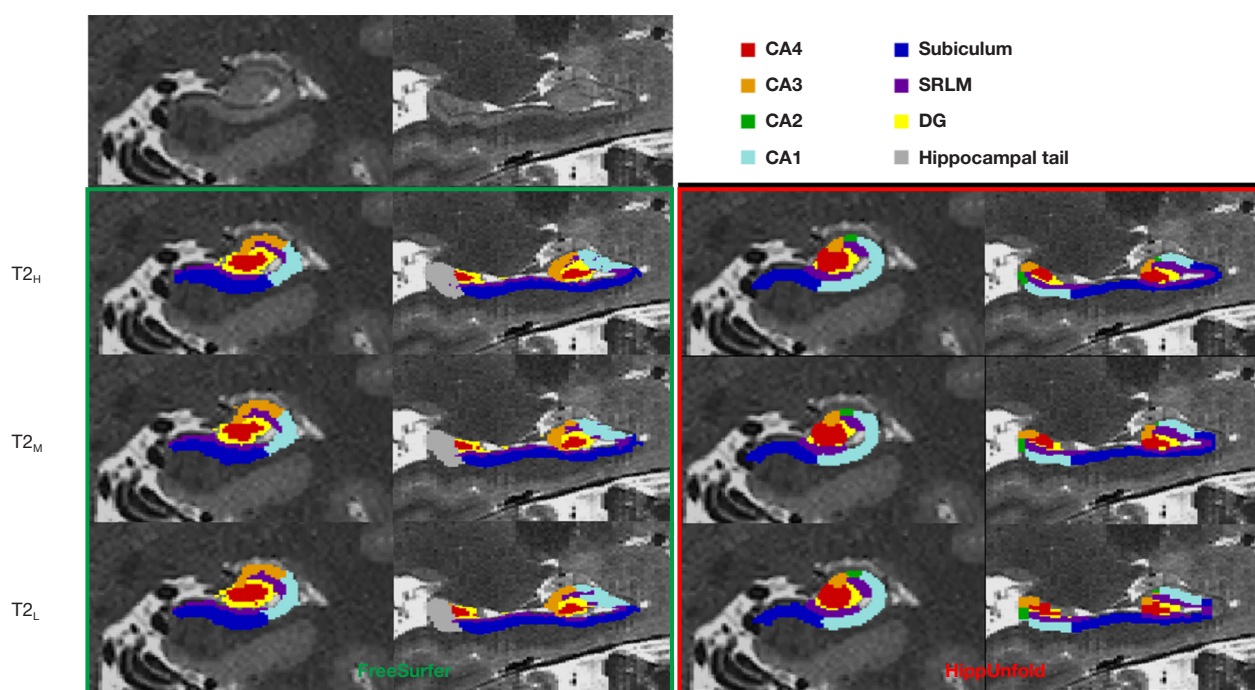
Figure 8 Subregion segmentation of the hippocampus from FreeSurfer (green box) and HippUnfold (red box) in a single participant. CA2 was included in CA3 in the FreeSurfer results. Hippocampal subfields were segmented with hippocampal tail in HippUnfold, while the hippocampal tail was a subfield part in FreeSurfer. $T2_H$, $T2_M$, and $T2_L$: T2-weighted images with slice thickness of 0.7, 1, and 2 mm, respectively. CA, cornu ammonis; DG, dentate gyrus; SRLM, stratum radiatum, lacunosum, and moleculare.

of the hippocampal anatomy and facilitating SRLM delineation (30). Hence, we propose acquiring high-resolution images with thinner slice thickness when image quality meets the clinical diagnostic standards. In our study, the SRLM was distinctly visible even at 0.7 mm, indicating that a slice thickness range of 0.7–1 mm can be used for 5 T.

The comparative analysis of FreeSurfer and HippUnfold highlighted differences in SRLM segmentation efficacy (the hypointense region within the hippocampus in images). Regarding the variation of Dice coefficients of SRLM with slice thickness, FreeSurfer and HippUnfold exhibited opposing tendencies. HippUnfold exhibited progressive Dice coefficient improvement with reduced thickness while FreeSurfer exhibited significant performance degradation. These findings suggest that HippUnfold, despite only using T2-weighted images for hippocampal subregion segmentation, may be better equipped to manage thinner-slice images. This could potentially be due to HippUnfold's employment of a deep convolutional neural network based on the U-Net architecture for tissue classification in T2-weighted images, wherein the SRLM plays a role in defining the unfolding coordinate boundaries. Additionally, thinner

slices of T2-weighted images enhance slice coherence, enabling more accurate boundary definition and thus more precise tissue segmentation.

Although the integration of T2-weighted with T1-weighted images in FreeSurfer (version 6.0 and above) has been reported to outperform isolated high-resolution T1-weighted images for segmentation, our data indicated certain limitations in its performance with high-resolution images, as indicated by the variability in Dice coefficient for the SRLM. This deterioration in performance likely stems from the predefined Gaussian distribution parameters in FreeSurfer, which in turn affects the accuracy of computing voxel label probabilities via T2 contrast information. In other words, the results of FreeSurfer imply that better image quality and thinner slice thickness do not necessarily provide better segmentation results since they also depend on the algorithms of autosegmentation tools.

Notably, in this study, our primary focus was placed on analyzing the performance of the two automatic tools in segmenting the SRLM. Moreover, it should be emphasized that both HippUnfold and FreeSurfer might possess other potential sources of inaccuracy in different anatomical

Quant Imaging Med Surg 2025;15(5):3861-3874 | https://dx.doi.org/10.21037/qims-24-2169

3872

Zou et al. Segmentation of hippocampal subregion via 5-T MRI

regions or for other structures that are not related to the SRLM.

Limitations

Three limitations of the present study warrant consideration. First, manual segmentation does not delineate all subregions, primarily because it is extremely time-consuming (requiring up to 50 hours per subject) and relies heavily on the understanding of the geometric relationships of hippocampal subregions with only the Dice coefficients of the SRLM being compared. Additionally, the relatively small sample size, especially for 3-T data, and the lack of scan–rescan analysis might have adversely impacted the statistical power. Further studies with larger samples and reliability testing are needed to validate these observations and provide additional insights into ultrahigh-field hippocampal studies.

Conclusions

The 5-T MRI system presents a promising high-resolution platform for detailed SRLM segmentation. However, the automated segmentation tools evaluated in this study demonstrated certain limitations, particularly when applied to high-resolution imaging. Future research should focus on optimizing these tools to fully leverage the benefits of high-field MRI and enhance the precision and reliability of hippocampal subregion segmentation. Moreover, establishing standardized definitions for hippocampal subregions is crucial for enabling accurate comparisons between segmentation methods and deepening insights into hippocampal pathology.

Acknowledgments

The authors would like to thank the Molecular Imaging platform, Medical Research Center, and Peking Union Medical College Hospital, for supporting of this study. The authors would also like to thank Yuyan Chen, Hualu Han, and Simin Liu for their assistance in data acquisition and processing.

Footnote

Reporting Checklist: The authors have completed the STROBE reporting checklist. Available at https://qims.amegroups.com/article/view/10.21037/qims-24-2169/rc

References

1. Small SA, Schobel SA, Buxton RB, Witter MP, Barnes CA. A pathophysiological framework of hippocampal dysfunction in ageing and disease. Nat Rev Neurosci 2011;12:585-601.
2. Scoville WB, Milner B. Loss of recent memory after bilateral hippocampal lesions. J Neurol Neurosurg Psychiatry 1957;20:11-21.
3. Eldridge LL, Knowlton BJ, Furmanski CS, Bookheimer

SY, Engel SA. Remembering episodes: a selective role for the hippocampus during retrieval. Nat Neurosci 2000;3:1149-52.

4. Morris RG. Elements of a neurobiological theory of hippocampal function: the role of synaptic plasticity, synaptic tagging and schemas. Eur J Neurosci 2006;23:2829-46.

5. Epstein RA, Patai EZ, Julian JB, Spiers HJ. The cognitive map in humans: spatial navigation and beyond. Nat Neurosci 2017;20:1504-13.

6. Convit A, De Leon MJ, Tarshish C, De Santi S, Tsui W, Rusinek H, George A. Specific hippocampal volume reductions in individuals at risk for Alzheimer's disease. Neurobiol Aging 1997;18:131-8.

7. Jack CR Jr, Petersen RC, Xu YC, O'Brien PC, Smith GE, Ivnik RJ, Boeve BF, Waring SC, Tangalos EG, Kokmen E. Prediction of AD with MRI-based hippocampal volume in mild cognitive impairment. Neurology 1999;52:1397-403.

8. Princich JP, Donnelly-Kehoe PA, Deleglise A, Vallejo-Azar MN, Pascariello GO, Seoane P, Veron Do Santos JG, Collavini S, Nasimbera AH, Kochen S. Diagnostic Performance of MRI Volumetry in Epilepsy Patients With Hippocampal Sclerosis Supported Through a Random Forest Automatic Classification Algorithm. Front Neurol 2021;12:613967.

9. Knight S, McCutcheon R, Dwir D, Grace AA, O'Daly O, McGuire P, Modinos G. Hippocampal circuit dysfunction in psychosis. Transl Psychiatry 2022;12:344.

10. Steve TA, Gargula J, Misaghi E, Nowacki TA, Schmitt LM, Wheatley BM, Gross DW. Hippocampal subfield measurement and ILAE hippocampal sclerosis subtype classification with in vivo 4.7 tesla MRI. Epilepsy Res 2020;161:106279.

11. Haukvik UK, Tamnes CK, Söderman E, Agartz I. Neuroimaging hippocampal subfields in schizophrenia and bipolar disorder: A systematic review and meta-analysis. J Psychiatr Res 2018;104:217-26.

12. Wang L, Swank JS, Glick IE, Gado MH, Miller MI, Morris JC, Csernansky JG. Changes in hippocampal volume and shape across time distinguish dementia of the Alzheimer type from healthy aging. Neuroimage 2003;20:667-82.

13. Mueller SG, Stables L, Du AT, Schuff N, Truran D, Cashdollar N, Weiner MW. Measurement of hippocampal subfields and age-related changes with high resolution MRI at 4T. Neurobiol Aging 2007;28:719-26.

14. Bussy A, Plitman E, Patel R, Tullo S, Salaciak A, Bedford SA, Farzin S, Béland ML, Valiquette V, Kazazian C, Tardif

CL, Devenyi GA, Chakravarty MM; Alzheimer's Disease Neuroimaging Initiative. Hippocampal subfield volumes across the healthy lifespan and the effects of MR sequence on estimates. Neuroimage 2021;233:117931.

15. Evans TE, Adams HHH, Licher S, Wolters FJ, van der Lugt A, Ikram MK, O'Sullivan MJ, Vernooij MW, Ikram MA. Subregional volumes of the hippocampus in relation to cognitive function and risk of dementia. Neuroimage 2018;178:129-35.

16. Malykhin NV, Lebel RM, Coupland NJ, Wilman AH, Carter R. In vivo quantification of hippocampal subfields using 4.7 T fast spin echo imaging. Neuroimage 2010;49:1224-30.

17. Fischl B, Salat DH, Busa E, Albert M, Dieterich M, Haselgrove C, van der Kouwe A, Killiany R, Kennedy D, Klaveness S, Montillo A, Makris N, Rosen B, Dale AM. Whole brain segmentation: automated labeling of neuroanatomical structures in the human brain. Neuron 2002;33:341-55.

18. Romero JE, Coupé P, Manjón JV. HIPS: A new hippocampus subfield segmentation method. Neuroimage 2017;163:286-95.

19. DeKraker J, Köhler S, Khan AR. Surface-based hippocampal subfield segmentation. Trends Neurosci 2021;44:856-63.

20. Fischl B. FreeSurfer. Neuroimage 2012;62:774-81.

21. DeKraker J, Haast RAM, Yousif MD, Karat B, Lau JC, Köhler S, Khan AR. Automated hippocampal unfolding for morphometry and subfield segmentation with HippUnfold. Elife. 2022 Dec 15;11:e77945.

22. Mueller SG, Yushkevich PA, Das S, Wang L, Van Leemput K, Iglesias JE, Alpert K, Mezher A, Ng P, Paz K, Weiner MW; Alzheimer's Disease Neuroimaging Initiative. Systematic comparison of different techniques to measure hippocampal subfield volumes in ADNI2. Neuroimage Clin 2017;17:1006-18.

23. Yushkevich PA, Amaral RS, Augustinack JC, Bender AR, Bernstein JD, Boccardi M, et al. Quantitative comparison of 21 protocols for labeling hippocampal subfields and parahippocampal subregions in in vivo MRI: towards a harmonized segmentation protocol. Neuroimage 2015;111:526-41.

24. Iglesias JE, Augustinack JC, Nguyen K, Player CM, Player A, Wright M, Roy N, Frosch MP, McKee AC, Wald LL, Fischl B, Van Leemput K; . A computational atlas of the hippocampal formation using ex vivo, ultra-high resolution MRI: Application to adaptive segmentation of in vivo MRI. Neuroimage 2015;115:117-37.

25. Chiappiniello A, Tarducci R, Muscio C, Bruzzone MG, Bozzali M, Tiraboschi P, et al. Automatic multispectral MRI segmentation of human hippocampal subfields: an evaluation of multicentric test-retest reproducibility. Brain Struct Funct 2021;226:137-50.

26. Cong S, Risacher SL, West JD, Wu YC, Apostolova LG, Tallman E, Rizkalla M, Salama P, Saykin AJ, Shen L. Volumetric comparison of hippocampal subfields extracted from 4-minute accelerated vs. 8-minute high-resolution T2-weighted 3T MRI scans. Brain Imaging Behav 2018;12:1583-95.

27. Yushkevich PA, Pluta JB, Wang H, Xie L, Ding SL, Gertje EC, Mancuso L, Kliot D, Das SR, Wolk DA. Automated volumetry and regional thickness analysis of hippocampal subfields and medial temporal cortical structures in mild cognitive impairment. Hum Brain Mapp 2015;36:258-87.

28. Pohmann R, Speck O, Scheffler K. Signal-to-noise ratio and MR tissue parameters in human brain imaging at 3, 7, and 9.4 tesla using current receive coil arrays. Magn Reson Med 2016;75:801-9.

29. Ver Hoef LW, Williams FB, Kennedy RE, Szaflarski JP, Knowlton RC. Predictive value of hippocampal internal architecture asymmetry in temporal lobe epilepsy. Epilepsy Res 2013;106:155-63.

30. Ver Hoef L, Deshpande H, Cure J, Selladurai G, Beattie J, Kennedy RE, Knowlton RC, Szaflarski JP. Clear and Consistent Imaging of Hippocampal Internal Architecture With High Resolution Multiple Image Co-registration and Averaging (HR-MICRA). Front Neurosci 2021;15:546312.

31. Dietrich O, Raya JG, Reeder SB, Reiser MF, Schoenberg SO. Measurement of signal-to-noise ratios in MR images: influence of multichannel coils, parallel imaging, and reconstruction filters. J Magn Reson Imaging 2007;26:375-85.

32. Carmichael DW, Thomas DL, De Vita E, Fernández-Seara MA, Chhina N, Cooper M, Sunderland C, Randell C, Turner R, Ordidge RJ. Improving whole brain structural MRI at 4.7 Tesla using 4 irregularly shaped receiver coils. Neuroimage 2006;32:1176-84.

33. Duan G, Zhao X, Anderson SW, Zhang X. Boosting magnetic resonance imaging signal-to-noise ratio using magnetic metamaterials. Commun Phys 2019;2:35.

34. Kwok WE. Basic Principles of and Practical Guide to Clinical MRI Radiofrequency Coils. Radiographics 2022;42:898-918.

35. Yan X, Ran L, Zou L, Luo Y, Yang Z, Zhang S, Zhang S, Xu J, Huang L, Xia L. Dark blood T2-weighted imaging of the human heart with AI-assisted compressed sensing: a patient cohort study. Quant Imaging Med Surg 2023;13:1699-710.